

## Accepted Manuscript

Investigation of the role of vacancy sources and sinks on the Kirkendall-effect on the nanoscale

J. Tomán, C. Cserháti, Y. Iguchi, Zs. Jánosfalvi, Z. Erdélyi

PII: S0040-6090(15)00523-4  
DOI: doi: [10.1016/j.tsf.2015.04.089](https://doi.org/10.1016/j.tsf.2015.04.089)  
Reference: TSF 34327

To appear in: *Thin Solid Films*



Please cite this article as: J. Tomán, C. Cserháti, Y. Iguchi, Zs. Jánosfalvi, Z. Erdélyi, Investigation of the role of vacancy sources and sinks on the Kirkendall-effect on the nanoscale, *Thin Solid Films* (2015), doi: [10.1016/j.tsf.2015.04.089](https://doi.org/10.1016/j.tsf.2015.04.089)

This is a PDF file of an unedited manuscript that has been accepted for publication. As a service to our customers we are providing this early version of the manuscript. The manuscript will undergo copyediting, typesetting, and review of the resulting proof before it is published in its final form. Please note that during the production process errors may be discovered which could affect the content, and all legal disclaimers that apply to the journal pertain.

# Investigation of the role of vacancy sources and sinks on the Kirkendall-effect on the nanoscale

J. Tomán, C. Cserhádi, Y. Iguchi, Zs. Jánosfalvi, Z. Erdélyi

*Department of Solid State Physics, University of Debrecen, P. O. Box. 2, H-4010 Debrecen, Hungary*

---

## Abstract

It is well-known that Kirkendall shift occurs in binary systems. We investigated diffusion on the nanometer scale in the framework of our conceptual model [Erdélyi and Schmitz, *Acta. Mater.* 60 (2012) 1807]. Since on this lengthscale the characteristic distances between the vacancy sources/sinks can be comparable to the dimensions of the sample, the usual vacancy annihilation processes, leading to the Kirkendall shift, cannot operate. In this situation, we studied the Kirkendall shift in planar geometry in case of miscible and restrictedly miscible systems by computer simulation.

*Keywords:* Kirkendall effect, diffusion, nanoscale, vacancy sources and sinks

---

## 1. Introduction

2 Since its discovery in 1947, the Kirkendall effect has played an important  
3 role in the development of solid state diffusion theory. Ernest Kirkendall in  
4 his third and last paper in a series [1, 2, 3] on the diffusion of Zn in  $\alpha$ -brass  
5 presented the results of his diffusion couple experiment. He electroplated a  
6 brass-bar with pure copper, but before that he placed inert Mo-wires along

7 each of the two surfaces to mark the original interfaces of the diffusion couple.  
8 After heat treatments of different times cross sections of the diffusion couple  
9 were investigated and Kirkendall found that the wires shifted inwards moving  
10 parabolically with the annealing time. He explained this observation with  
11 that the Zn-atoms move much faster outwards than the Cu-atoms inwards,  
12 causing the inner brass to shrink. The first theoretical description was made  
13 by Darken [4] using independent diffusion fluxes for the different constituents.  
14 Based on these results, Seitz [5] and Bardeen [6] showed from atomistic point  
15 of view, that the interdiffusion accompanied by vacancy mechanism lead to  
16 Darken's equations if it is assumed that the vacancy concentration is in local  
17 equilibrium. Vacancies should be created on one side and annihilated on the  
18 other side of the diffusion couple for the Kirkendall effect to occur.

19 The manifestation of the Kirkendall effect, besides the marker movement,  
20 can be the appearance of diffusional porosity (Kirkendall voids [7, 8]), gen-  
21 eration of stresses [8, 9] and the deformation of the whole specimen on the  
22 macroscopic scale [10]. Hollow nanoshell and nanowire formation was also  
23 explained by the Kirkendall effect [11, 12, 13].

24 In this study we are presenting a finite volume method to describe the  
25 interdiffusion process, as well as the Kirkendall effect on the nanoscale.

## 26 **2. Diffusion fundamentals**

27 As it is clear from Kirkendall's work, the effect can be best visualized by  
28 the motion of inert markers placed along the diffusion zone. The intrinsic  
29 diffusion fluxes of the components  $j_i$  [mol/m<sup>2</sup>s], which reflect the mobilities of  
30 the different species involved in the interaction, are then defined with respect

31 to this array of markers, called the Kirkendall frame of reference:

$$j_i = -D_i \frac{\partial C_i}{\partial x}. \quad (1)$$

32 Here  $D_i[m^2/s]$  is the intrinsic diffusion coefficient,  $C_i[mol/m^3]$  is the concen-  
33 tration of component  $i$  and  $x[m]$  is the position parameter. In case of an A-B  
34 binary diffusion couple the equations for the intrinsic fluxes are:

$$j_A = -D_A \frac{V_B}{V_m^2} \frac{\partial N_A}{\partial x}, \quad j_B = -D_B \frac{V_A}{V_m^2} \frac{\partial N_B}{\partial x}, \quad (2)$$

35 where  $N_i$  is the mole fraction of species A or B,  $V_m [m^3/mol]$  is the molar  
36 volume,  $V_i [m^3/mol]$  are the partial molar volumes of the different atoms  
37 [14, 15]. The latter is found through the tangent construction in the  $V_m$  vs.  
38  $N_i$  plot [16].

39 In writing Eq.(1) we followed the traditional Fick's approach, where the  
40 atomic flux is related to the gradient of the concentration (in moles per unit  
41 volume). There are of course more advanced methodes using the Onsager flux  
42 expressions for the intrinsic atomic fluxes that involve transport coefficients  
43 and thermodynamic forces acting on the atomic species. In this case the  
44 gradient of concentration is replaced with the corresponding gradient of mole  
45 fraction as required by the expression for the thermodynamic forces [17, 18].

46 The marker velocity depends on the difference in intrinsic diffusivities of  
47 the species and the concentration gradient developing in the diffusion zone  
48 at the marker plane composition [4]:

$$v = -(V_B j_B + V_A j_A) = -V_B (D_A - D_B) \frac{\partial C_B}{\partial x}. \quad (3)$$

49 In these calculations it is always supposed that only a volume diffusion con-  
50 trolled process operates. If this is the case, the inert markers positioned at

51 the original interface between the reactants are the only markers that stay at  
 52 a constant composition and move parabolically in time ( $x^2 \propto t$  or  $x \propto t^{1/2}$ )  
 53 during the whole interdiffusion process. The velocity of these markers is:

$$v_K = \frac{dx}{dt} = \frac{x_K}{2t}, \quad (4)$$

54 where  $x_K$  is the position of the Kirkendall plane. The location of the Kirk-  
 55 endall plane in the diffusion zone can be found graphically as the intersection  
 56 between the marker velocity plot  $2tv$  vs.  $x$  and the straight line  $2tv_K = x_K$   
 57 given by Eq.(4). In order to draw the line  $2tv_K = x_K$ , one needs to know  
 58 the position of the plane in the diffusion zone where the inert markers were  
 59 located at the beginning of the diffusion process, i.e. at time  $t = 0$ . However, if  
 60 the total volume of the specimen does not change during the interdiffusion,  
 61 this position can be determined by the usual Boltzmann-Matano method  
 62 [14, 15]. This kind of measurement allows us to determine the intrinsic dif-  
 63 fusion coefficients at a single composition, namely that of the Kirkendall  
 64 marker plane. To extend the measurement over the entire concentration  
 65 range, a so-called multifoil diffusion technique has been introduced [19, 20].  
 66 The characteristic feature of such a sample is, that each end-member of the  
 67 diffusion couple is composed of several thin foils with fiducial markers in be-  
 68 tween. Interdiffusion in such a multilayered sample will cause the markers  
 69 to move relative to the laboratory-fixed frame of reference. In the particular  
 70 case of [20],  $20\mu\text{m}$  Pd and  $21\mu\text{m}$  thick Ni foils were used with  $\text{ThO}_2$  powder  
 71 as fiducial markers (the diameter of the oxide particles were  $\sim 0.5 - 1\mu\text{m}$ ).  
 72 By measuring the shift of the markers, the Kirkendall displacement was de-  
 73 termined over the entire concentration range and the displacement curve was  
 74 constructed. Cornet [21, 22] and later van Loo [23] proposed a method to

75 obtain the Kirkendall velocity and then the intrinsic diffusion coefficient from  
 76 the displacement curve. It was found to be:

$$v = \frac{1}{2t} \left( y - x_o \frac{dy}{dx_o} \right), \quad (5)$$

77 with  $x_o$  being the original location of the markers at  $t = 0$ ,  $y$  is the dis-  
 78 placement of the markers, i.e.  $y = x - x_o$  and  $t$  is the annealing time. As it is  
 79 clear from Eq. (5), the position of the Kirkendall plane, as marked by inert  
 80 markers placed at the initial interface ( $x_o = 0$ ), is given by  $v_K = y/2t$  ( $v_K$  is  
 81 the velocity of the markers placed at the initial contact interface). This also  
 82 means that the Kirkendall plane can be found graphically as the intersection  
 83 between the marker velocity plot (Eq.(5)) and the straight line ( $2tv_K = x_K$ ),  
 84 supposing that at  $t = 0$  time the markers were at  $x_o = 0$ .

85 In this study we are modeling the above described phenomenon. Based  
 86 on our conceptual model [24], a one dimensional finite volume method was  
 87 developed. The planar sample was divided into  $n$  slabs ( $n = 2000$ ), where  
 88 each slab mimics a metallic foil in the above described multifoil experiment.  
 89 Note, that the number of the slabs only influences the spatial resolution of  
 90 the calculated concentration profiles. In each computational cycle the total  
 91 number of atoms transported between the neighboring slabs were calculated  
 92 from which the change of composition as well as the thickness of the slab  
 93 were determined. During the calculations the walls of the slabs are taken  
 94 as markers in a multifoil experiment. From the calculations we get the dis-  
 95 placement curve by registering the positions of the cell walls and the number  
 96 of computation cycles. The velocity curve was calculated from Eq.(5) as a  
 97 usual procedure in case of multifoil experiments.

98 For the computer simulation a simplified version of the model described

99 in [24] was implemented. In that work a complete set of analytical equations  
 100 was developed in order to describe reactive diffusion in spherical core shell  
 101 nanostructures. The model takes into account elastic stress, its plastic re-  
 102 laxation, as well as possible non-equilibrium vacancy densities. Furthermore,  
 103 thermodynamic driving forces are included to model formation of intermetal-  
 104 lic product phases in intermediate composition range. Here we use the planar  
 105 version of these equations (see the Appendix A. in [24]). In addition the effect  
 106 and the change of the molar volume during the interdiffusion as well as the  
 107 consequences of the developing stresses were neglected. On the other hand,  
 108 considering that the vacancy concentration changes due to atomic fluxes as  
 109 well as due to the activity of vacancy sinks and sources, the continuity equa-  
 110 tion written in the Kirkendall reference system contains the vacancy flux  
 111 and the term of vacancy sources and sinks as well. Including these terms  
 112 into Fick's second law we arrive at:

$$\frac{\partial N_i}{\partial t} = -V_m(\nabla j_i x + N_i S_v), \quad (6)$$

113 where  $S_v[mol \cdot m^{-3} \cdot s^{-1}]$  is the vacancy source term, i.e. the number of  
 114 vacancies created in unit volume per unit time. This expression is very  
 115 similar to [17, 18]. We define  $s_v$  as:

$$s_v = S_v \cdot V_m = K_r(C_v^o - C_v), \quad (7)$$

116 which is the rate of change of the atomic fraction of vacancies due to cre-  
 117 ation/annihilation.  $K_r[1/s]$  determines the effectiveness of sinks and sources,  
 118 therefore  $s_v$  is proportional to the deviation of the vacancy concentration  
 119 from it's equilibrium value. Note that  $K_r$  may vary with spatial coordinates,  
 120 depending on the spatial distribution of the sinks and sources. Since  $K_r$  is a

121 function of space, the solution of the diffusion equation, i.e. the movement  
122 of the inert markers will not follow the so called parabolic law. (Note that  
123 taking constant  $K_r$  the solution adheres to the traditional parabolic time  
124 evolution.) Another effect which may alter the parabolic behaviour of the  
125 diffusion process is the finite size of the sample. When the diffusion profile  
126 reaches the end of the diffusion couple, the kinetic of the process is changing.

### 127 3. Results of the computer simulation

128 The algorithm and the selection of the input parameters were similar to  
129 the ones in [24]. Several cases have been studied. In order to validate our  
130 calculations we performed simulations using the parameters given in [20, 25].  
131 The intrinsic diffusivities were concentration dependent, but the ratio of the  
132 diffusivities was constant ( $D_A/D_B = \text{const.}$ ). The interdiffusion coefficient  
133 ( $\tilde{D} = C_B V_B D_A + C_A V_A D_B$ ) was also constant in the whole concentration  
134 range. Studies have been completed in ideal solid solutions with vacancy  
135 sinks and sources active enough in every cell of the one dimensional finite vol-  
136 ume model to maintain equilibrium vacancy concentration during the whole  
137 process. Fig. 1. displays a representative plot showing that our model safely  
138 reproduces the calculations, implemented in the traditional Darken's model  
139 [25], as well as the experimental observations reported in [25]. The scale on  
140 the horizontal and vertical axes are in arbitrary units on the figures. The  
141 dashed and the solid lines mark the displacement and the velocity curve  
142 respectively. The straight line represents the ( $2tv_K = x_K$ ) equation. The  
143 interdiffusion coefficients published in [20] were used to calculate the concen-  
144 tration profiles and the corresponding Kirkendall displacement and velocity

145 curves. It can be clearly seen, that the displacement as well as the velocity  
146 curves are almost exactly follow the trace of the experimental data presented  
147 (displacement curve) on Fig.10. and the velocity curve on Fig.14. in [20].  
148 Fig. 1b. demonstrates the composition dependence of the diffusivities. Note  
149 the logarithmic scale on the vertical axis.

150 We extended our studies to immiscible systems too and also by chang-  
151 ing the arrangement of vacancy sources and sinks along the sample. Con-  
152 centration dependent diffusivities have been used with various composition  
153 dependence.

154 We simulated the diffusion process in which the diffusivities depend ex-  
155 ponentially on the concentration (for instance  $D_i = D_{io}exp(mN_i)$ , where  
156  $i = A$  or  $B$ ), moreover the ratio of the diffusivities are constant. Fig. 2a.  
157 shows the displacement (dashed line) as well as the velocity curve (solid red  
158 line) when the vacancy sources and sinks are evenly active in every slab  
159 (foil). On Fig. 2b. the same is plotted but with a different vacancy source  
160 and sink distribution. As it was mentioned before,  $K_r$  in Eq.(7) may vary  
161 along the sample. It was supposed that the vacancy sources and sinks are  
162 active enough in the slabs in the very vicinity of the starting interface to  
163 maintain the equilibrium vacancy concentration all the time ( $K_r = 1/s$ ) but  
164 beyond that their activities approach to zero following a Gaussian distribu-  
165 tion. For the sake of simplicity we will call this distribution of vacancy sinks  
166 and sources Gaussian in this paper (see the dot-dashed curve on Fig. 2b.).  
167 This is a practical assumption since there are always impurities at the contact  
168 plane. Fig. 2c. demonstrates the composition dependence of the diffusivities.  
169 Note the logarithmic scale on the vertical axis.

170 As it was expected based on the consideration of Philibert [15], the max-  
171 imum of the velocity curve and that of the displacement curve coincide with  
172 the position of the Kirkendall plane for the case of constant ratio of intrinsic  
173 diffusivities in both cases. On the other hand, the velocity curve in Fig. 2b.  
174 shows a local maximum at the Kirkendall plane (which in this case coincide  
175 with the Matano plane), the global maximum is more to the left. This means  
176 that although the Kirkendall plane is stable, the markers placed on positions  
177 where the gradient of the velocity curve is negative (left to the Kirkendall  
178 plane) get closer to each other during the process, which means another con-  
179 densation of the markers, which is different from the Kirkendall plane. In  
180 case of a system having a miscibility gap similar results were obtained. The  
181 maximum of the velocity curve and displacement curve in this case also co-  
182 incide with the position of the Kirkendall plane and altering the distribution  
183 of the sources and sinks to a Gaussian one, the velocity curve changes con-  
184 siderably, showing another local maximum, indicating similar behavior as in  
185 ideal solid solution.

186 Fig. 3a. shows again the displacement as well as the velocity curve when  
187 the vacancy sources and sinks are evenly active in every slab (foil) and in  
188 Fig. 3b. the result of a calculation with a Gaussian vacancy source and  
189 sink distribution is plotted. In this system an exponential concentration  
190 dependence of the intrinsic diffusion coefficients were supposed, no other  
191 constrain was taken into consideration, moreover there is also a miscibility  
192 gap ( $0.25 < N_A < 0.75$ ). It can be seen that the maximum of the Kirkendall  
193 velocity is situated at the Matano and not at the Kirkendall plane. On  
194 the other hand, the maximum of the displacement and the position of the

195 Kirkendall plane coincide. The same is true if we look at Fig. 3b, where the  
196 vacancy sources and sinks have different distribution. As can be seen, in this  
197 case as well there are other local maxima of the velocity curve, indicating  
198 again that the markers are getting closer to each other in the vicinity of  
199 these peaks. This practically would mean that the markers are "attracted"  
200 by these maxima implying three weak places along the diffusion direction.  
201 The shape of the reconstructed velocity curve on Fig. 2b. and Fig. 3b. are  
202 due to the space dependance of  $K_r$  effectiveness factor, as well as the finite  
203 size of the film

204 The presented plots so far showed only stable Kirkendall planes in a sense,  
205 that those markers which, at the end of the annealing, ended up slightly  
206 ahead of the intersection point of the velocity curve and the straight line  
207 ( $2tv_K = x_K$ ), would slow down (lower velocity) and if these markers were  
208 behind this plane, they would move faster (higher velocity). In other words,  
209 the plane located at the intersection point tends to attract inert markers in  
210 its vicinity.

211 According to [21, 22, 25], there is no reason why the maximum in the  
212 velocity curve, the maximum in the displacement curve and the Kirkendall  
213 plane should coincide. On Fig. 4a. we show a plot, where this is not the  
214 case. Moreover the Kirkendall plane in this case is unstable since, following  
215 the earlier argument, the markers which are slightly ahead of the Kirkendall  
216 plane, move faster and markers slightly behind this plane will migrate slower.  
217 Fig. 4b. demonstrates the composition dependence of the diffusivities.

218 Experimental verification of these ideas can be found in previous studies  
219 on diffusion phenomena and the Kirkendall effect in the  $\beta'$ -ordered AuZn

220 phase (B2 structure) of the binary Au-Zn system [26].

221 From these calculations it is clear that our model gives unexpected results  
222 concerning the position of the fiducial markers used in a so-called multifoil  
223 experiments. Applying real concentration dependent diffusivities and a spa-  
224 tial distribution of vacancy sinks and sources, even in these simple cases, we  
225 found, that there is indeed a Kirkendall plane which, by definition, is the  
226 plane that stays at a constant composition and moves parabolically in time  
227 during the whole interdiffusion process. On the other hand, there are other  
228 places in the diffusion zone which attract markers. That place or even those  
229 places do not move parabolically in time but, as the process goes further,  
230 attract more and more particles. As a result, such a place may become a  
231 problematic microstructural feature in any joint, because of higher mechan-  
232 ical failure risk at this plane.

#### 233 4. Conclusions

234 Interdiffusion on the nanometer scale was investigated in the framework  
235 of our conceptual model [24]. We studied the Kirkendall shift in planar  
236 geometry in case of miscible and restrictedly miscible systems by computer  
237 simulation. A one dimensional finite volume method was developed, in which  
238 the sample was divided into  $n$  slabs. The slabs mimicked the foils in the so  
239 called multifoil experiment. From the calculations we get the displacement  
240 as well as the velocity curves by registering the position of the cell walls  
241 and the number of computation cycles. Calculations were performed in two  
242 different distribution of vacancy sources and sinks i.e.: the sources and sinks  
243 are distributed evenly in the whole sample, or they followed a Gaussian

244 distribution, having the maximum at the location of the Kirkendall plane.

245 It is clear that our results, concerning the position of the cell walls which  
246 act as markers in a multifoil experiment, are different from the earlier ones.  
247 Applying realistic situations, like concentration dependent diffusivities as well  
248 as spatial distribution of vacancy sinks and sources, even in very simple cases  
249 it was found that besides the Kirkendall plane there are other places in the  
250 interdiffusion specimen which attract markers. Markers placed to positions  
251 where the gradient of the velocity curve gets negative during the process  
252 get closer to each other as time goes on, resulting another condensation of  
253 the markers, which is different from the Kirkendall plane. That place, or  
254 even those places do not move parabolically in time but, as the process  
255 goes further, attract more and more particles, getting weaker and weaker in  
256 mechanical point of view.

## 257 5. Acknowledgement

258 This work was supported by the OTKA Board of Hungary (No. NF101329),  
259 by the TAMOP 4.2.2.A-11/1/KONV- 2012-0036 and TAMOP-4.2.2/B-10/1-  
260 2010-0024 projects (implemented through the New Hungary Development  
261 Plan co-financed by the European Social Fund, and the European Regional  
262 Development Fund). The authors appreciate the help of Mark van Dal pro-  
263 viding his experimental data presented in [20, 25]

## 264 References

- 265 [1] E. Kirkendall, L. Thomassen, C. Upthegrove, Rates of Diffusion of Cop-  
266 per and Zinc in Alpha Brass, Trans. AIME 133 (1939) 186–203.

- 267 [2] E. O. Kirkendall, Diffusion of Zinc in Alpha Brass, Trans. AIME 147  
268 (1942) 104–110.
- 269 [3] A. D. Smigelskas, E. O. Kirkendall, Zinc Diffusion in Alpha Brass, Trans.  
270 AIME 171 (1947) 133–142.
- 271 [4] L. S. Darken, Diffusion, mobility and their interrelation through free  
272 energy in binary metallic systems, Trans. AIME 175 (1948) 184–201.
- 273 [5] F. Seitz, On the Theory of Vacancy Diffusion in Alloys, Phys. Rev. 74  
274 (1948) 1513–1523.
- 275 [6] J. Bardeen, Diffusion in Binary Alloys, Phys. Rev. 76 (1949) 1403–1405.
- 276 [7] Y. A. Geguzin, M. A. Krivoglaz, Motion of Macroscopic Inclusions in  
277 Solids, Nauka (in russian) (1979) 215.
- 278 [8] D. L. Beke, Z. Erdélyi, I. A. Szabó, Nonlinear Stress Effects in Diffusion,  
279 Defect Diffus. Forum 264 (2007) 117–122.
- 280 [9] G. B. Stephenson, Deformation during interdiffusion, Acta Metall.  
281 Mater. 36 (1988) 2663–2683.
- 282 [10] I. Daruka, I. A. Szabó, D. L. Beke, C. Cserhádi, A. A. Kodentsov, F. J. J.  
283 van Loo, Diffusion-induced bending of thin sheet couples: Theory and  
284 experiments in Ti-Zr system, Acta. Mater. 44 (1996) 4981–4993.
- 285 [11] A. M. Gusak, T. V. Zaporozhets, K. N. Tu, U. Gösele, Kinetic analysis  
286 of the instability of hollow nanoparticles, Philos. Mag. 85 (36) (2005)  
287 4445–4464.

- 288 [12] G. E. Murch, A. V. Evteev, E. V. Levtheke, I. V. Belova, Recent  
289 Progress in the Simulation of Diffusion Associated with Hollow and Bi-  
290 Metallic Nanoparticles, *Diff. Fund.* 42 (2009) 1–22.
- 291 [13] C. Cserháti, G. Glodán, D. L. Beke, Hollow hemisphere formation by  
292 pure Kirkendall porosity, *Diff. Found.* 1 (2014) 61–73.
- 293 [14] P. G. Shewmon, *Diffusion in Solids*, McGraw-Hill Book Company, USA,  
294 1963.
- 295 [15] J. Philibert, *Atom Movements, Diffusion and Mass Transport in Solids*,  
296 Les Editions de Physique, Les Ulis, France, 1991.
- 297 [16] R. A. Swalin, *Thermodynamics of Solids*, John Wiley & Sons, Inc., New  
298 York, 1972.
- 299 [17] J. Svoboda, F. Fischer, P. Fratzl, Diffusion in multi-component systems  
300 with no or dense sources and sinks for vacancies, *Acta Mater.* 50 (2002)  
301 1369–1381.
- 302 [18] J. Svoboda, F. Fischer, P. Fratzl, Diffusion and creep in multi-  
303 component alloys with non-ideal sources and sinks for vacancies, *Acta*  
304 *Mater.* 54 (2006) 3043–3053.
- 305 [19] T. Heumann, G. Walther, Der Kirkendall-Effekt in Silber-Gold-  
306 Legierungen im gesamten Konzentrationsbereich, *Z. Metallkd.* 48 (1957)  
307 151.
- 308 [20] M. J. H. van Dal, M. C. L. P. Pleumeekers, A. A. Kodentsov, F. J. J.

- 309 van Loo, Intrinsic diffusion and Kirkendall effect in Ni-Pd and Fe-Pd  
310 solid solutions, *Acta. Mater.* 48 (2000) 385–396.
- 311 [21] J. F. Cornet, D. Calais, Etude de leffect Kirkendall dapres les equations  
312 de Darken, *J. Phys. Chem. Solids.* 33 (1972) 1675–1684.
- 313 [22] J. F. Cornet, Complements a letude de leffect Kirkendall selon les equa-  
314 tions de Darken, *J. Phys. Chem. Solids.* 35 (1974) 1247–1252.
- 315 [23] F. J. J. van Loo, G. F. Bastin, G. D. Rieck, Marker displacements as a  
316 result of diffusion in binary metal systems, *Sci. Sint.* 11 (1979) 9–27.
- 317 [24] Z. Erdélyi, G. Schmitz, Reactive diffusion and stress in spherical geom-  
318 etry, *Acta. Mater.* 60 (2012) 1807–1817.
- 319 [25] M. J. H. van Dal, Microstructural stability of the Kirkendall plane,  
320 Eindhoven :Technische Universiteit Eindhoven, 2001, phd thesis edn.,  
321 2001.
- 322 [26] M. J. H. van Dal, A. M. Gusak, C. Cserhádi, A. A. Kodentsov, F. J. J.  
323 van Loo, Spatio-temporal instabilities of the Kirkendall marker planes  
324 during interdiffusion in  $\beta'$ -AuZn, *Philos. Mag. A* 82 (5) (2002) 943–954.

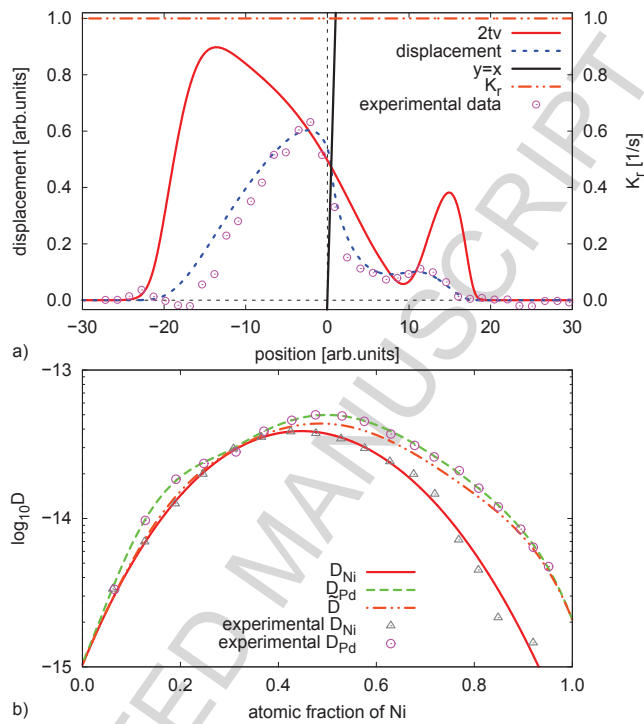


Figure 1: Representative plot, showing the validity of our model. The displacement (dashed line) and the velocity curve (solid red line) on plot (a) are the same as in Fig. 10. and Fig. 14. in [20]. Plot(b) shows the concentration dependence of the interdiffusion coefficient, as well as the intrinsic diffusivities of the different species. The experimental data-points are replotted from [20].

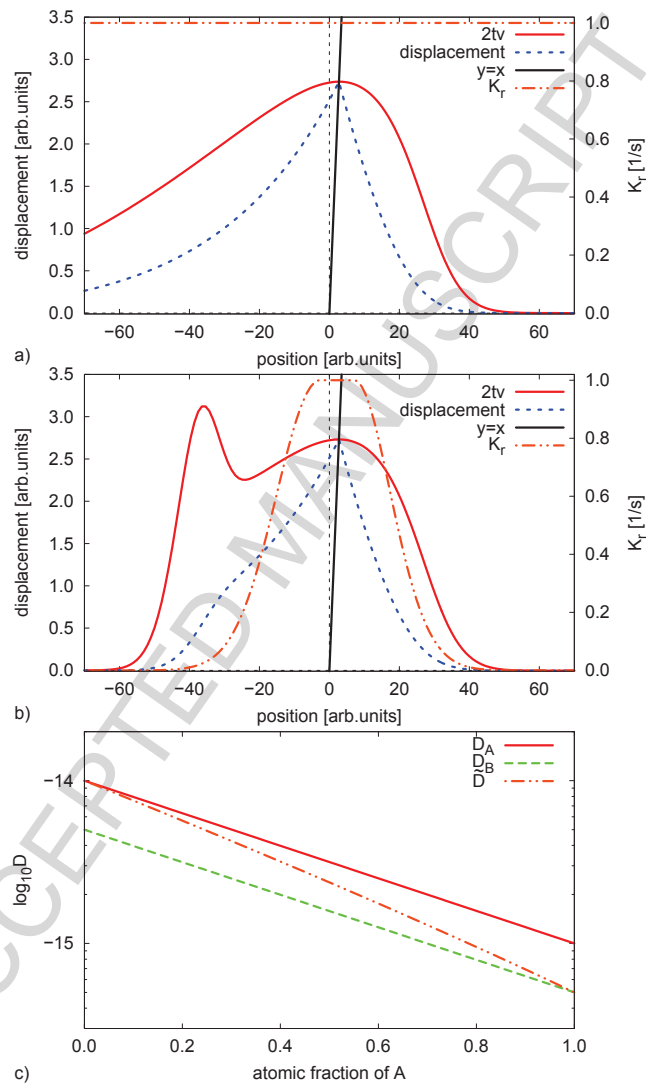


Figure 2: In case of ideal solid solution plot (a) shows the displacement (dashed line) as well as the velocity curve (solid red line) when the vacancy sources and sinks are evenly active at every slab. On plot (b) the same is presented but with a Gaussian vacancy source and sink distribution (dot-dashed line, see the text). Plot (c) shows the concentration dependence of the diffusivities of the different species.

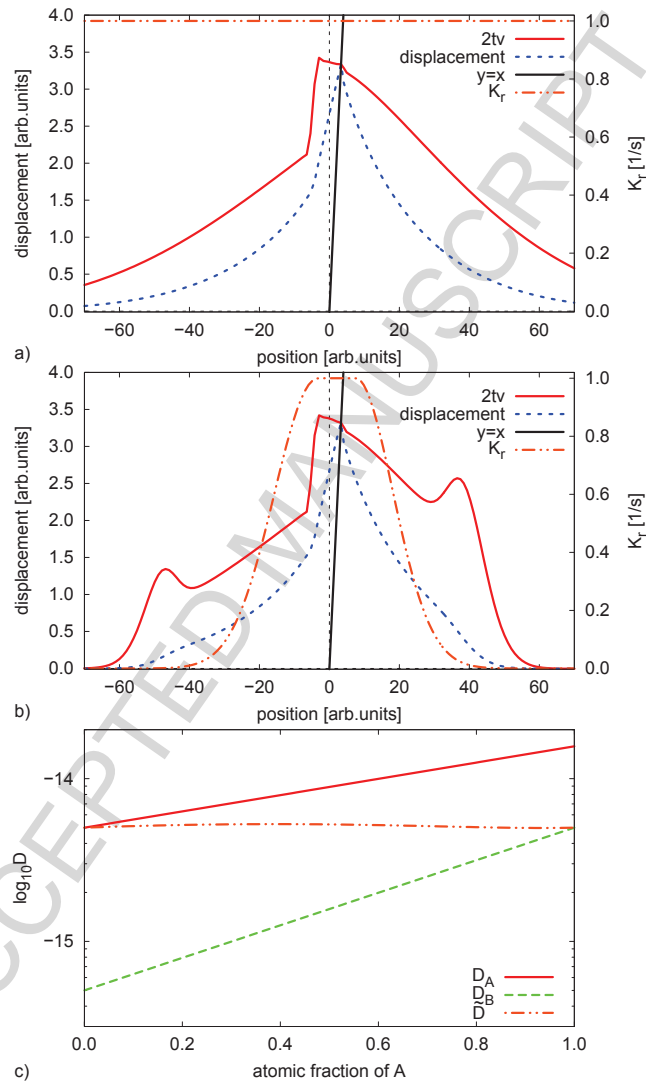


Figure 3: In case of a solid solution with a miscibility gap, plot (a) shows the displacement (dashed line) as well as the velocity curve (solid red line) when the vacancy sources and sinks are evenly active at every slab. In plot (b) the same is presented but with a Gaussian vacancy source and sink distribution (dot-dashed line). Plot (c) shows the concentration dependence of the diffusivities of the different species.

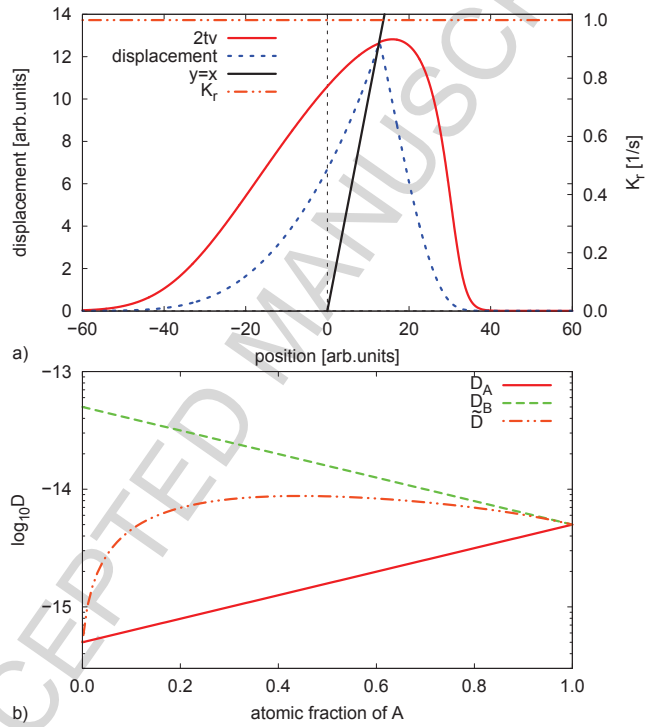


Figure 4: On plot (a) the maximum of the Kirkendall velocity (solid red line) is situated at the Matano and not at the Kirkendall plane. In this calculation  $K_r = 1$  in every slab. The Kirkendall plane is unstable in this case (see the text). Plot (b) shows the concentration dependence of the diffusivities of the different species.

## Highlihgts

- Interdiffusion was investigated on the nanometer scale using computer simulation.
- Kirkendall shift was studied in planar geometry in different binary systems.
- The calculations are validated by simulations using the parameters of Ni/Pd system.
- We show other places in the interdiffusion zone which attract markers.